Color–Selected High Redshift Galaxies and the HDF

By Mark Dickinson

The Johns Hopkins University and STScI

The quality, depth, and multi–color nature of the Hubble Deep Field images makes them an excellent resource for studying galaxies at $z > 2$ using selection techniques based on the presence of the 912Å Lyman break. I present a descriptive review of this method and of the properties of the objects which it identifies, and summarize spectroscopic progress on galaxies with $2 < z < 4$ in the HDF. Using ground–based and HDF samples of Lyman break galaxies I discuss the luminosity function of galaxies at $z \approx 3$, and consider the effects of extinction on the star formation rates that are derived from the UV luminosity information. Infrared observations of the HDF provide data on the rest–frame optical properties of $z \approx 3$ galaxies, which are briefly described.

1. Introduction

Although the study of galaxies at high redshift neither begins nor ends with the Hubble Deep Field (HDF), this conference has demonstrated the ways in which the HDF has served to focus the attention of the community on the properties of galaxies at $z > 2$. In part this is because the HDF imaging data was obtained through several filters, permitting the use of color selection techniques to isolate and study populations of galaxies at various redshifts. Because the HDF images are so deep, colors can be measured with unusually high precision (and in a spatially resolved fashion *within* individual galaxies) for objects which ordinarily would be considered very faint for ground–based telescopes. Additionally, the HDF images easily detect galaxies at magnitudes well beyond the spectroscopic limits of even the largest telescopes. The desire to understand their nature requires *some* idea of their distances, and it is therefore tempting to look for photometric means of estimating redshifts without the benefit of ordinary spectroscopy.

For these reasons, many presentations at this symposium have considered various applications of "photometric redshift" estimation in the HDF and in other data sets. One such method takes advantage of the ubiquitous 912Å Lyman limit discontinuity, which is redshifted into the HDF bandpasses at $z \gtrsim 2$. In recent years, color selection based on the Lyman limit has developed into a highly successful means of detecting galaxies at large redshifts, as I will review below. In designing the HDF observations, our working group at STScI incorporated F300W imaging into the four–filter scheme for two reasons, one scientific and one purely practical. First, such data offers the potential for Lyman break selection of high redshift galaxies. Second, we wished to take advantage of the "bright" portions of the orbit during Continuous View Zone visibility, when scattered earthlight severely impacts WFPC2 imaging at redder wavelengths. The reduced amplitude of the scattered background at UV wavelengths, and the fact that F300W imaging with WFPC2 is not normally background limited anyway, made bright–time observing through that bandpass a suitable use for these otherwise disadvantageous observing intervals.

I begin with a descriptive review of the Lyman break technique, illustrated using data from the HDF. Although the HDF Lyman break galaxy sample is much smaller than that which has been identified from ground–based imaging studies (which cover much larger solid angles), the excellent photometric precision of the HDF data and the large percentage of Lyman break galaxies present at the fainter magnitude limits which it

probes makes it quite useful for illustrating the principles of the method. In §2.1 I summarize the current status of spectroscopy on HDF Lyman break galaxies. In §3 I discuss some of the statistical properties of Lyman break galaxies, concentrating on their numbers, luminosities, and colors, and inferences that can be derived from these measurements. Finally, §4 discusses the rest–frame optical properties of $z > 2$ galaxies in the HDF using deep infrared imaging data. In his contribution to this volume, Mauro Giavalisco discusses our ground–based Lyman break galaxy sample in greater detail, and addresses the spectroscopic, morphological, and clustering properties of Lyman break galaxies, which I will largely neglect here.

In this paper, HDF galaxy selection and object names are based on the catalog of Williams et al. (1996). Optical photometry is reported on the AB magnitude system, with the WFPC2 bandpasses indicated by U_{300}, B_{450}, V_{606} and I_{814}. In general I have used new, revised photometry of the Williams et al. catalog objects based on optimized apertures which maximize signal–to–noise for color measurement. This has the advantage of allowing robust Lyman break galaxy selection to somewhat fainter magnitudes than was previously possible.

2. Lyman break selected galaxies in the HDF

Figure 1 illustrates the principle of the Lyman break color selection technique using a galaxy from the HDF as an example. In the absence of dust extinction, an actively star–forming galaxy should have a blue continuum at rest–frame ultraviolet wavelengths, nearly flat in f_ν units. Blueward of the 912Å Lyman limit, however, photoelectric absorption by intervening sources of neutral Hydrogen will sharply truncate the spectrum. This hydrogen may be located in the photospheres of the UV–emitting stars themselves, in the interstellar medium of the distant galaxy, or along the intergalactic sightline between us and the object. When observed at some large redshift, the rest–frame Lyman limit of a galaxy shifts between some pair of bandpasses (e.g. the WFPC2 U_{300} and B_{450} filters in figure 1), and the galaxy "drops out" when viewed through the bluer filter because of the suppression of its flux. In addition to the Lyman continuum absorption, the cumulative effect of the Lyman α forest lines introduces an additional spectral break shortward of Lyman α at the emission redshift of the galaxy. This flux suppression is increasingly strong at higher redshifts as the forest thickens, and introduces its own color effects, particularly for galaxies at $z > 3$.

Color selection based on the effects of the Lyman limit and Lyman α forest has been used for many years in surveys for distant QSOs (e.g. Warren et al. 1987). The method was applied to the study of distant galaxies by Guhathakurta et al. (1990) and Songaila, Cowie & Lilly (1990), who used it set limits on the number of star–forming galaxies at $z \approx 3$ in faint galaxy samples. Steidel & Hamilton (1992) and Steidel, Hamilton & Pettini (1995) reported the detection of significant numbers of high redshift galaxy candidates using this method. Spectroscopic confirmation of their redshifts was first presented by Steidel et al. (1996a), and WFPC2 images of select examples were published by Giavalisco et al. (1996b). To date, the majority of Lyman break selected galaxies come from the $U_nG\mathcal{R}$ survey of Steidel et al., which has identified more than a thousand candidates and has spectroscopically confirmed (as of this writing) more than 400 galaxies at $z \approx 3$. This survey is discussed in greater detail by Giavalisco in this volume, and in the present paper I will often refer to it as the "ground–based sample" to distinguish it from HDF–selected objects.

Although Lyman break galaxies in the HDF are fewer in number than those in the ground–based sample, the quality and depth of the HDF imaging data offer a number

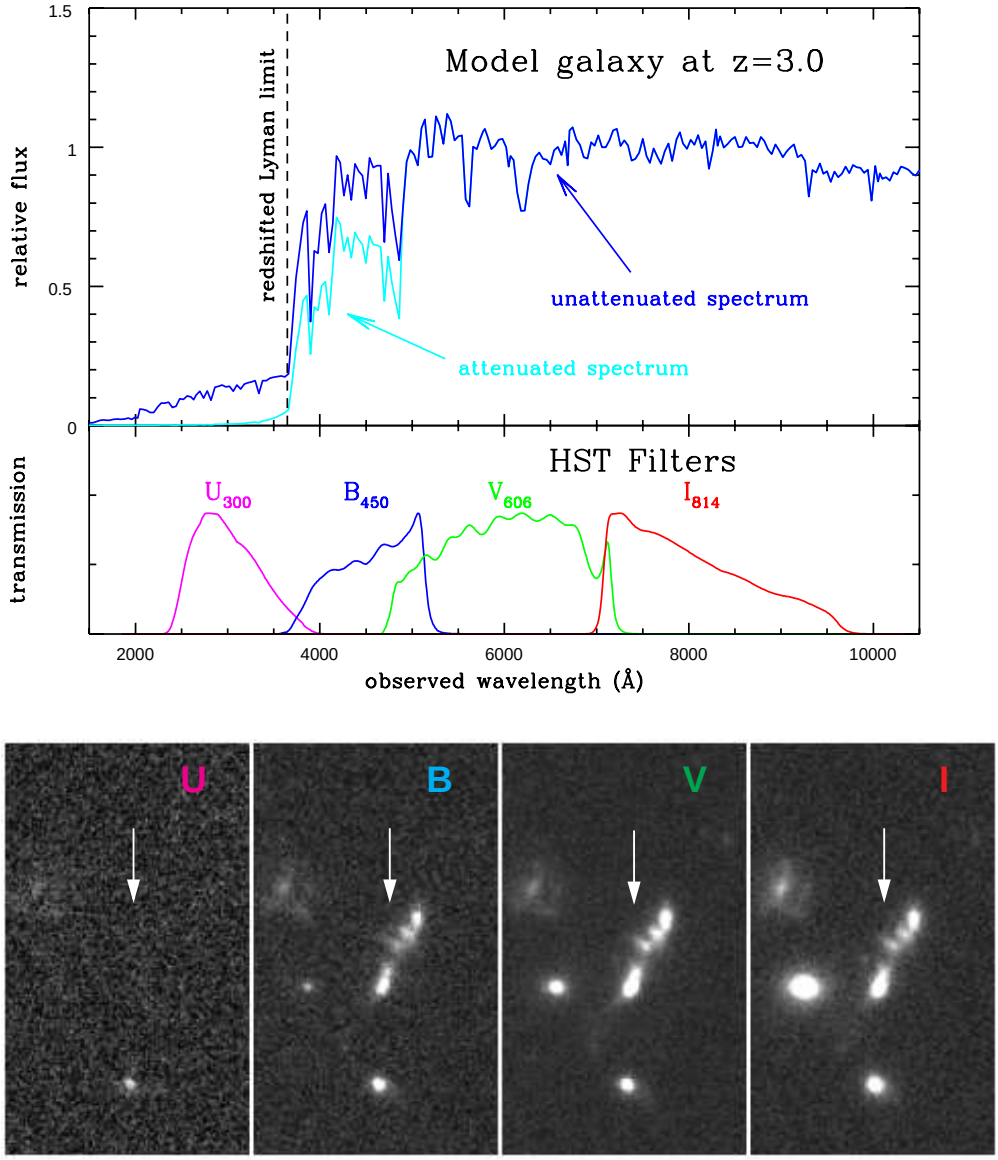

FIGURE 1. Illustration of the Lyman break technique as applied to the Hubble Deep Field. The upper panel shows a model spectrum of a star forming galaxy observed at $z = 3$. Its flat UV continuum is truncated by the 912Å Lyman limit, which is redshifted between the U_{300} and B_{450} filters (WFPC2 bandpasses shown below spectrum). In addition to photospheric absorption in the UV–emitting stars, the effects of intergalactic neutral hydrogen further suppress the continuum in the U_{300} and B_{450} bands. At bottom, an HDF galaxy is shown in the four WFPC2 bandpasses. Clearly visible at I_{814}, V_{606} and B_{450}, it vanishes in the U_{300} image. This galaxy has been spectroscopically confirmed to have $z = 2.8$.

of advantages. The HDF can be used to detect Lyman break galaxies at fainter apparent magnitudes than has been achieved in ground–based data, and the precision of the B_{450}, V_{606} and I_{814} photometry ensures small random errors on color measurements. Moreover, the depth and resolution of the WFPC2 imaging permits detailed morphological study of these objects. The primary *disadvantage* of the HDF is its small field

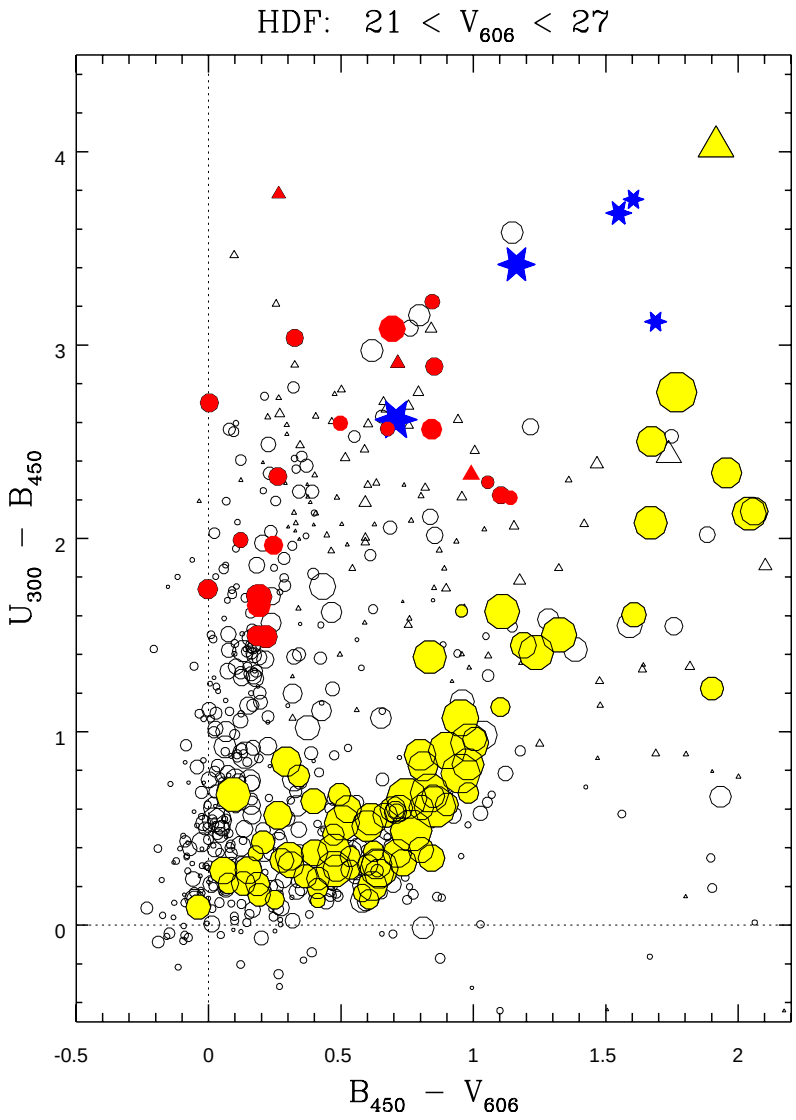

FIGURE 2. Color–color diagram of faint galaxies in the Hubble Deep Field, illustrating the "plume" of Lyman break objects rising from $U_{300} - B_{450} = B_{450} - V_{606} = 0$. These are nearly all galaxies at $z > 2$. Spectroscopically confirmed objects in this redshift range are shown as darker filled symbols; galaxies with measured redshifts $z < 2$ are shown as light filled circles, and stars are indicated by star–shaped points. Triangles mark lower limits (1σ to the $U_{300} - B_{450}$ color for objects undetected in U_{300}. Symbol size scales inversely with apparent V_{606} magnitude.

of view, and hence the rather small comoving volume which it samples. This limits its utility for statistical studies (e.g. of luminosity functions, redshift distributions, etc.), as small number statistics, galaxy clustering, and field–to–field variations may introduce significant uncertainties.

2.1. *Color selection of Lyman break galaxies in the HDF*

My own favorite "view" of the Hubble Deep Field is that shown in figure 2, a color–color diagram of galaxies in the HDF. One of the most prominent features of this diagram is the dramatic "plume" of galaxies rising nearly vertically from the zero color point (i.e. flat spectrum galaxies) up toward very red $U_{300}-B_{450}$ colors. These are the high redshift, star forming galaxies – objects whose 912Å Lyman discontinuities are entering into and passing through the F300W bandpass, shifting them into a portion of color–color space which is unpopulated by low redshift objects.

Figure 3 illustrates the redshift dependent effect of the Lyman limit and Lyman α spectral "breaks" on the colors of galaxies with spectroscopically confirmed redshifts $z > 2$. To first order, the galaxies in the high redshift "plume" form a redshift sequence ordered by $U_{300}-B_{450}$ color. In practise, variation in individual galaxy spectra shuffle this sequence somewhat. Dynamic range for the U_{300} photometry also affects this ordering, as it is only possible to set limits on the $U_{300} - B_{450}$ colors of fainter objects, and the numerical values of these limits therefore depend on the apparent magnitude of the galaxies. The lower panel of figure 3 shows the increasing effect of the Lyman α forest (and, at $z \gtrsim 3.5$, of the Lyman limit) on the B_{450} - V_{606} color. This effect was used by Lowenthal et al. (1997) as an additional criterion for identifying high redshift galaxy candidates (cf. also Fruchter, this volume). Using color selection criteria such as those of Steidel et al. (1996a,b; see also below), the application of a color cut such as $B_{450} - V_{606} \leq 1.2$ results in an upper redshift bound $z \lesssim 3.5$. It is this reddening of $B_{450} - V_{606}$ which is responsible for the "tilt" of the plume in the UBV color–color diagram shown in figure 2 – the higher redshift U_{300} dropout galaxies "fan out" toward redder B_{450} - V_{606} colors. Figure 4 shows a different 2–color diagram of HDF galaxies, this time using V_{606} - I_{814} colors which are relatively unaffected by Lyα absorption at $z < 4$. Here, the "plume" remains more or less vertical.

The Lyman break color technique is a simple form of photometric redshift selection. Here we do not attempt to accurately estimate the redshifts of individual objects, but simply to use color criteria to select galaxies in a particular redshift interval and exclude foreground (and background) objects. The redshift selection function of the method depends on the particular color criteria adopted, on the intrinsic dispersion in the ultraviolet spectral properties of star forming, high redshift galaxies, on cosmic variance in the intergalactic transmission along different lines of sight, and on the distribution of photometric measurement errors. This redshift selection function can be estimated using spectral models along with realistic simulations of photometric errors, or can be measured directly by obtaining enough spectroscopic redshifts to define it empirically. We now know that the Lyman break galaxy population exhibits strong clustering in redshift space (Steidel et al. 1998; cf. also Giavalisco, this volume, and figure 7 below). Therefore in order to determine the redshift selection function empirically one must study many independent sightlines in order to average over the effects of large scale structure. We have done this for our ground–based survey, and thus feel that we understand the redshift selection function quite well. For the HDF, we have only the one "realization" of the redshift distribution, and thus the empirical selection function cannot properly be determined – here we must rely to some degree on models, although these models can be informed by the information on galaxy spectral properties which has been gained from the ground–based samples.

The F300W filter in WFPC2 is substantially bluer than U bandpasses used at terrestrial observatories. As such, U_{300} photometry is sensitive to the passage of the Lyman break at significantly lower redshifts than is the case for, e.g., the $U_nG\mathcal{R}$ system used by

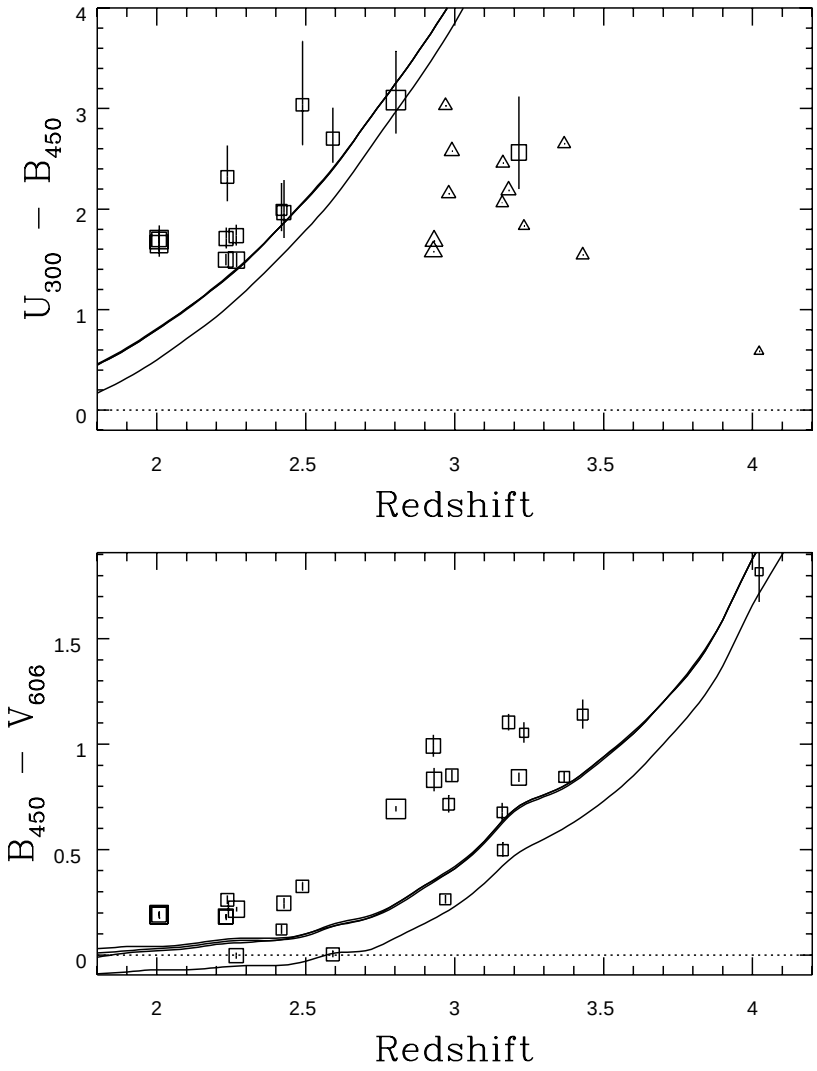

FIGURE 3. U_{300} - B_{450} and B_{450} - V_{606} versus redshift for spectroscopically confirmed $z > 2$ galaxies in the HDF. These plots illustrate the effect of Lyman limit and Lyman α absorption on the colors of high redshift galaxies. The solid lines show predicted colors of actively star–forming galaxies of various sorts using the Madau (1995) prescription for mean intergalactic transmission. In the top panel, triangles mark lower color limits for galaxies with $S/N < 2$ in the U_{300} band. All galaxies with $z < 2.9$ are detected in U_{300}, while all but one galaxy with $z > 2.9$ have $S/N < 2$. (The exception, 4-858.0, is formally detected with $S/N \approx 2.5$; this may partially result from the red leak in the U_{300} filter or from systematic measurement error, but could also indicate photometric contamination from a foreground object.) The lower panel shows the progressive reddening of the B_{450} - V_{606} color with redshift, primarily due to the effect of the Lyman α forest. (Compare with figure 10 for galaxies from the ground–based sample.)

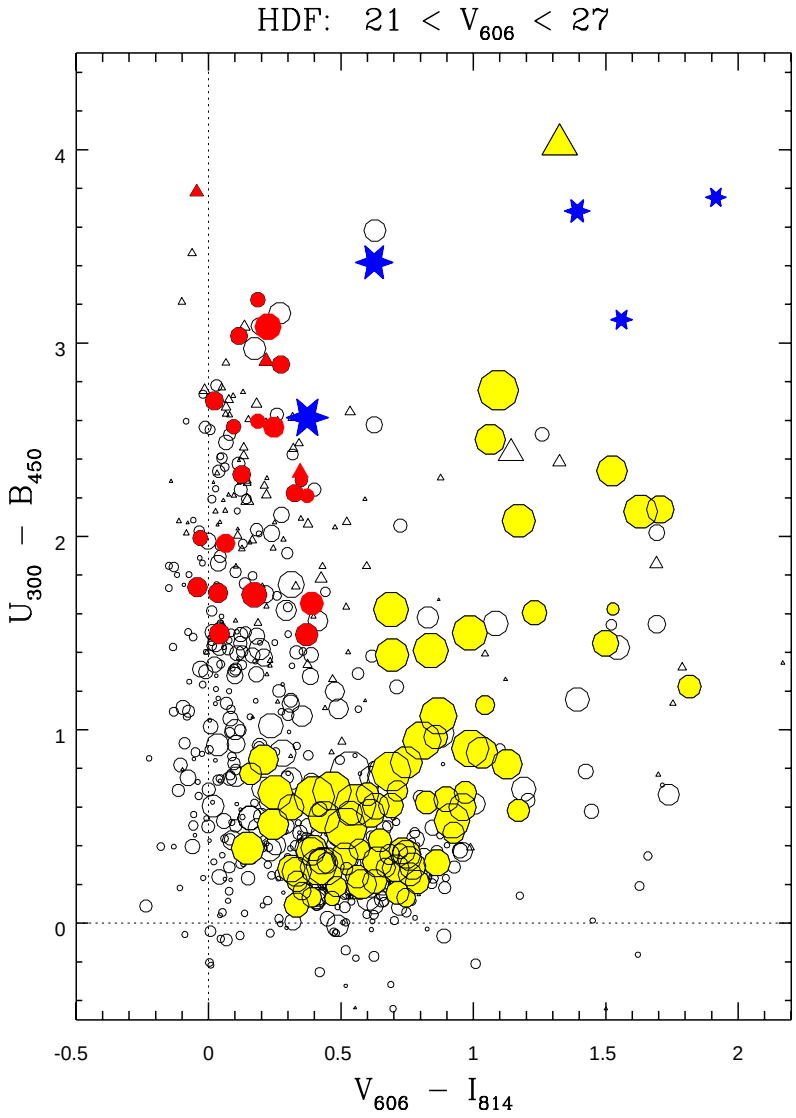

FIGURE 4. Another multi–color view of the HDF. Here, the horizontal axis plots the $V_{606} - I_{814}$ color, which is relatively insensitive to intergalactic Lyman α absorption for redshifts $z < 4$. In this particular multi–color space the "plume" of high redshift galaxies stands nearly vertical, without the tilt seen in figure 2. Symbols are the same as in figure 2.

Steidel et al. For example, roughly 90% of galaxies in our ground–based $U_n G\mathcal{R}$ survey lie in the redshift range $2.6 < z < 3.4$. By $z = 2$, however, the Lyman limit is already well into the WFPC2 F300W bandpass and produces a recognizably large color signature. Followup spectroscopy has already identified U_{300}–dropout galaxies down to $z = 2.01$, and others which did not successfully yield redshifts quite likely lie at redshifts slightly below 2, where the absence of strong spectral features in the wavelength range presently accessible to LRIS at Keck makes secure redshift measurement difficult. The commis-

sioning of a new blue channel on LRIS will soon make it possible to measure redshifts for many more U_{300} dropouts in the HDF.

The sensitivity of the U_{300} filter to Lyman break galaxies at lower redshifts has benefits and disadvantages. It opens a larger volume of redshift space to Lyman break selection, thus increasing the number of objects which may be identified this way. At the same time, as already noted, it makes many of them more difficult to confirm with optical spectra. However, the ease of selecting galaxies at $2 < z < 2.5$ has one spectroscopic advantage: this is the range of "magic redshifts" for near–infrared spectroscopy, where the [OII], [OIII], Hβ and Hα lines are all accessible in the J, H and K bands. This may make the HDF Lyman break galaxies particularly useful for studying nebular emission line diagnostics; already Elston et al. have observed Hα from several HDF Lyman break galaxies at $z \approx 2$ (see below).

Various groups have created photometrically defined samples of high redshift galaxy candidates in the HDF. The color selection criteria differ, and no "definitive" method has yet been established. The number of Lyman break candidates therefore varies from sample to sample depending on the criteria which are adopted. For example, Madau et al. (1996) defined conservative selection criteria based on models of galaxy color distributions in order to select $z > 2$ galaxies while avoiding significant risk of contamination from objects at lower redshift. These criteria, however, miss some of the galaxies which are now spectroscopically confirmed to have $z > 2$. Using the wealth of redshift information now available in the HDF we can revisit this question and refine the selection criteria. As it happens, applying the same criteria used by Steidel et al. for selecting Lyman break galaxies in the ground–based $U_n G\mathcal{R}$ color system does an excellent job of isolating $z > 2$ galaxies in the HDF. Specifically, we may use the so–called "marginal" criteria of Steidel et al., namely

$$U_{300} - B_{450} \geq B_{450} - V_{606} + 1.0, \qquad B_{450} - V_{606} \leq 1.2.$$

This successfully recovers all 24 spectroscopically confirmed Lyman break galaxies in the HDF at $2 < z < 3.5$. As is the case for the ground–based sample, the only substantial contaminants are galactic stars, some of which also satisfy these criteria, but these are easily recognized in the WFPC2 images and excluded. (All obvious stars with these colors have also already been observed spectroscopically, as it turns out.) The only known low–redshift galaxy which satisfies these criteria is, of all things, the brightest galaxy in the HDF: an elliptical in WF2 at $z = 0.089$. This is not surprising, as ellipticals have colors similar to those of K–stars, and are thus "interlopers" for the same reason until their redshifts become large enough ($z \approx 0.1$) for k–correction effects to move them out of the color selection region. There should be very few $z < 0.1$ early–type galaxies in the small volume of the HDF which populate this part of color–color space.†

Excluding stars and the few obvious $z < 0.1$ interlopers, there are approximately 187 galaxies in the HDF with $V_{606} < 27.0$ which satisfy these color criteria and thus probably fall in the redshift range $2 \lesssim z \lesssim 3.5$. The exact number depends somewhat on the choice of what constitutes a single galaxy with multiple clumps versus separate objects with small angular separations. E.g. should the "quad galaxy," 4–858.0 at $z = 3.22$, be considered a single galaxy with four pieces or four separate objects? Such distinctions may be merely semantic or may be very important depending on the question being asked (cf. Colley et al. (1996)).

† For those particularly worried about foreground contamination, an additional color cut, $V_{606} - I_{814} \leq 0.5$, should successfully exclude most interlopers at $z < 0.1$.

HDF Galaxies with Spectroscopic Redshifts $z > 2$

ID	RA	Dec	z	V_{606}	Reference
2-449.0	12:36:48.332	62:14:16.67	2.008	23.68	S
2-585.1	12:36:49.808	62:14:15.18	2.008:	23.85	E
3-118.1	12:36:54.724	62:13:14.74	2.232	24.41	*
2-903.0	12:36:55.071	62:13:47.05	2.233	24.60	L
2-525.0	12:36:50.120	62:14:01.04	2.237	24.80	*
2-82.1	12:36:44.077	62:14:09.98	2.267	24.54	L
4-445.0	12:36:44.637	62:12:27.34	2.268	24.08	C
2-824.0	12:36:54.617	62:13:41.28	2.419	25.23	L
2-239.0	12:36:45.883	62:14:12.10	2.427	24.54	*
2-591.2	12:36:53.175	62:13:22.76	2.489	24.91	*
4-639.1	12:36:41.715	62:12:38.84	2.591	24.74	S
4-555.1	12:36:45.344	62:11:52.67	2.803	23.41	S
1-54.0	12:36:44.094	62:13:10.75	2.929	24.44	*
4-52.0	12:36:47.687	62:12:55.98	2.931	24.37	L
4-289.0	12:36:46.944	62:12:26.09	2.969	25.17	*
4-363.0	12:36:48.297	62:11:45.88	2.980	25.05	L
2-643.0	12:36:53.427	62:13:29.38	2.991	24.87	L
2-76.11	12:36:45.357	62:13:46.98	3.160	25.32	L
2-565.0	12:36:51.186	62:13:48.79	3.162	25.17	*
2-901.0	12:36:53.607	62:14:10.25	3.181	24.87	L
4-858.0	12:36:41.233	62:12:03.00	3.216	24.28	S,L,Z
3-243.0	12:36:49.817	62:12:48.88	3.233	25.60	L
3-577.0	12:36:52.247	62:12:27.18	3.360	27.25	Z
2-637.0	12:36:52.747	62:13:39.08	3.368	25.27	L
2-604.0	12:36:52.407	62:13:37.68	3.430	25.25	L
3-512.0	12:36:56.117	62:12:44.69	4.022	25.85	*

References

S: Steidel et al. 1996b; L: Lowenthal et al. 1997; C: Cohen et al. 1996;
Z: Zepf et al. 1997; E: Elston et al. private communication;
*: this paper (Steidel et al. observations, unpublished)

2.2. *HDF high–z roundup*

To date, 26 galaxies in the HDF have spectroscopic redshifts $z > 2$. 23 of these were pre–selected as Lyman break objects for spectroscopic observation. One galaxy, 4-445.0, was observed by Cohen et al. (1996) as part of a magnitude limited spectroscopic sample, but qualifies photometrically as a Lyman break galaxy nevertheless. One other was was observed serendipitously (2-585.1 – see below), but also satisfies the Lyman break color criteria defined above. Finally, one galaxy (3-577.0) was observed as a gravitational lens candidate; it is too faint for a robust U_{300} Lyman break measurement and so does not qualify (see below). Table 1 lists these objects, including several galaxies from our own observations which are previously unpublished. There are many more Lyman break candidates, primarily U_{300} dropouts, which have spectroscopically accessible magnitudes, and with considerable effort this list could eventually more than double in length. Few of the B_{450} dropout objects ($z \sim 4$ candidates) are bright enough to tempt the spectroscopist, but if they have strong emission lines a few may still yield redshifts.

Here are a few notes on individual Lyman break galaxies, including corrigenda to some errors in our first paper on HDF spectroscopy (Steidel et al. 1996b).

2-449.0: This galaxy was erroneously identified as having $z = 2.845$ in Steidel et al. 1996b (object C2-05 in that paper). The broad band spectral energy distribution of the galaxy, both in the UV and near–IR, appears to be inconsistent with that redshift (e.g. the Lyman break amplitude is too small for the galaxy to be at $z = 2.8$). We reanalyzed the spectrum and found that $z = 2.008$ is more likely to be the correct redshift. The galaxy was then observed by Elston et al. in the infrared to search for Hα emission, both with narrow band imaging at the IRTF and with the Cryogenic Spectrograph (CRSP) at KPNO. Both observations detected strong line emission, confirming the new redshift.

2-585.1: This galaxy, a U_{300} Lyman break galaxy with a particularly dramatic morphology (see figure 15 below), lies several arcseconds away from 2-449.1 (see above). In their CRSP observations of 2-449.1, Elston et al. also detected line emission from 2-585.1 which fortuitously fell on their spectrograph slit. The line was confirmed with a subsequent observation targeting 2-585.1 itself. Presuming the line to be Hα, the redshift is approximately the same as that of 2-449.1. Both galaxies have very similar $U_{300} - B_{450}$ colors, again suggesting similar redshifts.

3-550.0: This galaxy, object C3-02 from Steidel et al. 1996b, is not included in the table above. As with 2-449.0 (above), the colors are in most respects not consistent with the published redshift ($z = 2.775$); the relatively small U_{300} - B_{450} color and near–IR SED both suggest a lower redshift. The original spectrum has very poor signal–to–noise, and we now feel that the published redshift is probably incorrect. Reobservations of this galaxy have thus far been inconclusive. We suspect that the galaxy has $z \lesssim 2$, making spectroscopic redshift confirmation difficult with LRIS at the present time.

3-577.0: This is the faintest object (with $V_{606} > 27$!) in the HDF with a reported redshift. Hogg et al. (1996) proposed that this is part of a gravitational lens system consisting of a red foreground elliptical, a large blue arc, and 3-577.0 as a suggested counterimage of the arc. Zepf et al. (1997) observed the system and detected a weak emission line from 3-577.0 which they interpret as Lyman α. Their spectra did not yield redshifts for the other components of the system. Although the emission line is very weak and the proposed redshift should perhaps be regarded as tentative, it is plausibly correct. 3-577.0 is too faint to be robustly measured as a "dropout," as the U_{300} photometry is not deep enough to set a strong enough constraint on the $U_{300} - B_{450}$ color. However, the colors are not *inconsistent* with it being at $z \sim 3$. Moreover, photometrically the "arc" (3-593.0) does qualify as a Lyman break galaxy, and probably has $z > 2$. Thus it remains plausible that the two objects are one and the same, gravitationally lensed. Arguing against this is the absence of any emission line in Zepf et al.'s spectrum of the arc, and the fact that the two objects have apparently different $B_{450} - V_{606}$ colors (although they are virtually identical at $V_{606} - I_{814}$). To explain this would require that the long slit observation, which crossed the arc perpendicularly, must simply have missed the line emitting region of the magnified galaxy. The $B_{450} - V_{606}$ colors, if the galaxies are at $z = 3.36$, could conceivably be affected by different amounts of foreground Lyman α forest absorption, while the $V_{606} - I_{814}$ colors are free of this effect. Further observations of this system are warranted.

3-512.0: Of the candidate $z \approx 4$ "B_{450}–dropouts" tabulated in Madau et al. 1996, only three objects have $I_{814} < 26$. 3-512.0 is the brightest of these at V_{606}. The galaxy is in fact detected in the B_{450} image, and does not drop out completely. If this is indeed a high redshift object, then the Lyman limit has only partially passed through the filter bandpass, suggesting $z \approx 4$. We observed this galaxy with LRIS at the Keck Observatory in May 1996 and again in March 1997. Both observations detected a single emission line at λ6105Å. If the emission line is identified with Lyman α, this would imply a redshift $z = 4.02$. No other significant lines were detected. In particular, if the observed line were

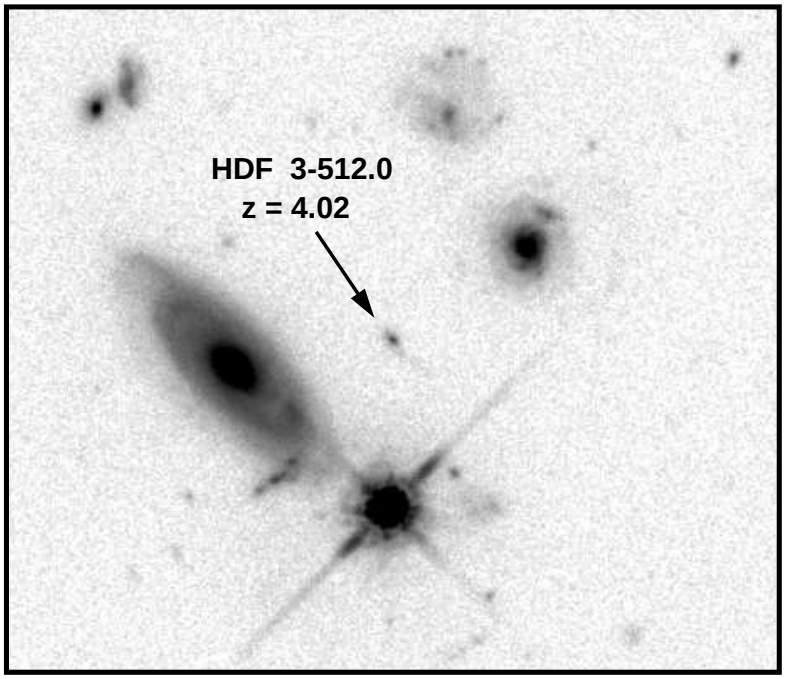

FIGURE 5. Image of 3-512.0, one of the brightest B_{450}–dropout galaxies in the HDF. A single emission line detected in its spectrum suggests that 3-512.0 has $z = 4.02$.

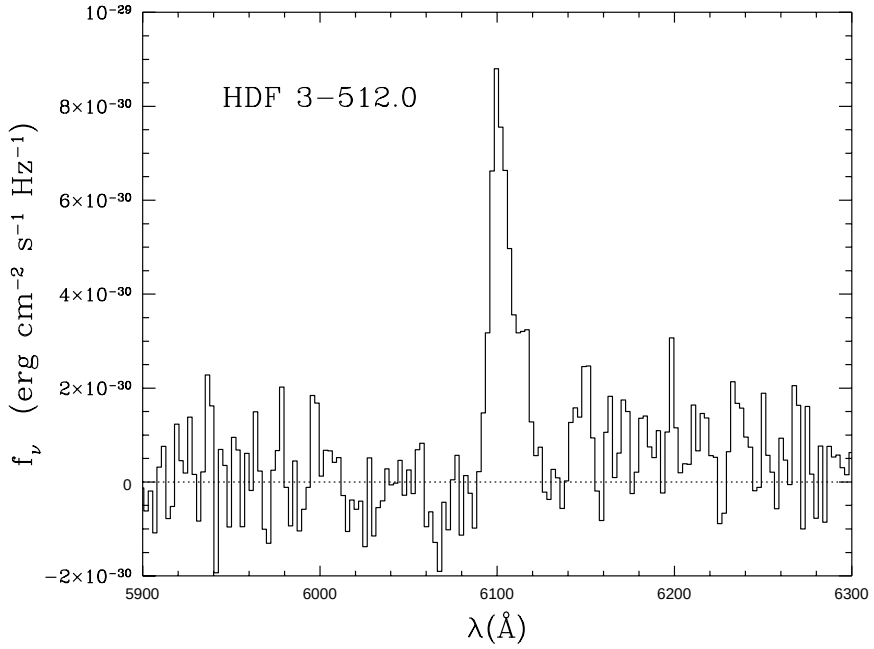

FIGURE 6. Spectrum of 3-512.0, showing the emission line detected at λ6105Å. The asymmetric line profile and the continuum discontinuity across the line are both consistent with this being Lyman α at $z = 4.02$.

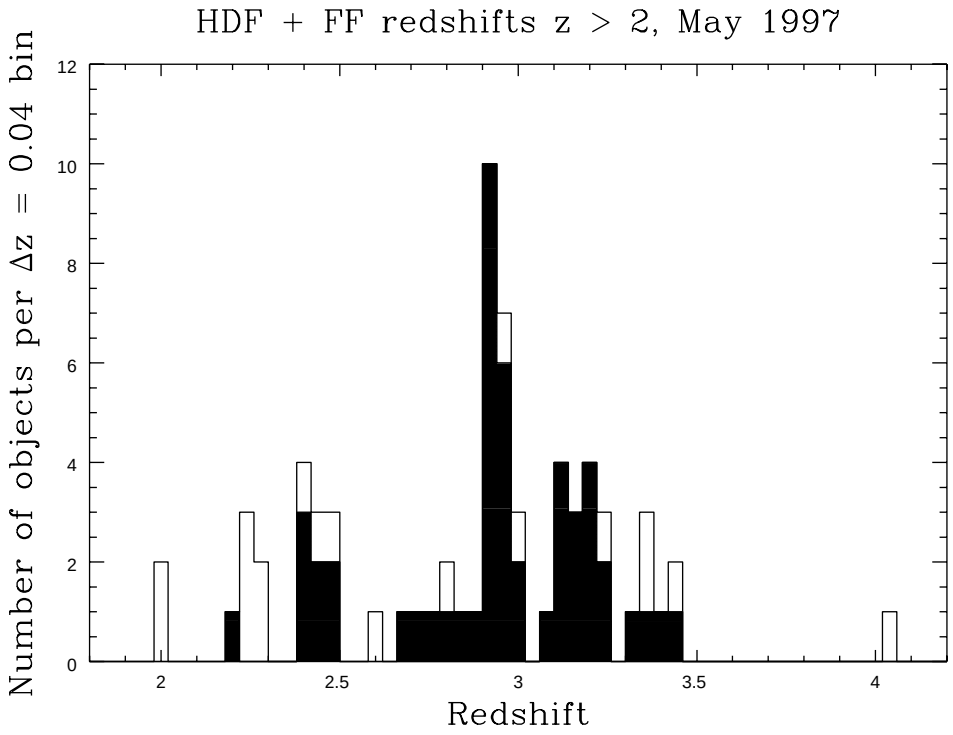

FIGURE 7. The overall redshift distribution of galaxies with $z > 2$ in the HDF and its Flanking Fields. The filled portion of the histogram are galaxies selected from our ground–based $U_nG\mathcal{R}$ imaging, primarily outside the central HDF, while the open histogram includes additional Lyman break galaxies in the central HDF.

[OII] λ3727Å or [OIII] λ5007Å from a low–redshift object our spectrum would cover the wavelength ranges where other strong optical lines are expected, and none are seen. The coincidence between color–selection as a "weak" B–dropout and the redshift derived on the assumption that the line is Lyman α is suggestive. The spectrum (see figure 6) shows a flux discontinuity across the emission line, as would be expected for a $z \approx 4$ galaxy due to intervening absorption from the Lyman α forest. Moreover, the emission line profile is asymmetric, with a sharp blue side and extended red wing. This characteristic profile is often seen in high redshift quasars and galaxies (cf. the $z = 4.9$ galaxy of Franx et al. (1997)), where it is due to absorption of the blue side of Lyman α by intervening neutral hydrogen. Although a single–line redshift cannot be regarded as 100% secure, the additional circumstantial evidence suggests that this is indeed a galaxy at $z = 4.02$.

As part of our general survey for Lyman break galaxies we have used the Palomar 200–inch telescope to image a wider region (roughly $9' \times 9'$) which includes the HDF and its flanking fields, selecting candidates using our standard $U_nG\mathcal{R}$ color criteria. The overall redshift distribution of $z > 2$ galaxies now known from the central HDF and the surrounding region is shown in figure 7. As has been often noted from surveys at $z < 1$, the redshift distribution in this narrow pencil beam is highly non–random, with prominent "spikes" where the galaxy density is large. The existence and significance of strong clustering in the Lyman break galaxy population is discussed in several papers

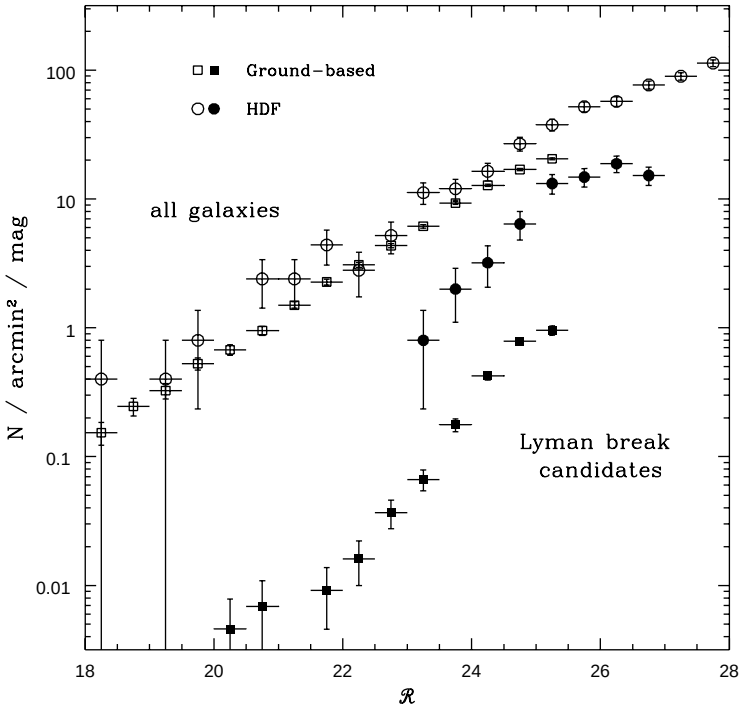

FIGURE 8. Number counts of Lyman break galaxies from ground–based and HDF samples compared to the overall counts of faint field galaxies. R magnitudes are approximated for HDF galaxies as $(V_{606} + I_{814})/2$.

now in press: Steidel et al. (1998) report on a strong redshift "spike" seen in another survey field, while Giavalisco et al. (1998; see also this volume) have measured the angular correlation function of Lyman break galaxies. Figure 7, as well as data we have collected in other fields, shows that these highly overdense redshift–space structures are ubiquitous at $z \approx 3$ – the case studied in Steidel et al. (1998) is not unique, and we find similar spikes in essentially all of our survey fields once sufficiently large numbers of redshifts have been collected. The HDF is no exception.

3. Statistics of Lyman break galaxies

What fraction of the faint galaxy population lies at these large redshifts? This was the question addressed by Guhathakurta et al. (1990), who were among the first to apply the Lyman break technique to faint galaxy samples. At the magnitude limits of their sample they found few U–band dropout objects and concluded that only a small fraction of faint galaxies lie at $z \approx 3$. However this fraction rises as we go fainter; the exact proportion depends on the color selection (different criteria probe different volumes at high redshift) and the photometric depth of the sample. In figure 8 I show the overall number counts of galaxies in our ground–based survey and in the HDF, compared to the number of Lyman break candidates in each. Brighter than $\mathcal{R} = 22.9$, all of the color–selected objects in the ground–based sample have turned out to be galactic stars (plus a small number of high redshift QSOs) – we have yet to find a Lyman break galaxy with $\mathcal{R} < 22.9$ in the

0.24 square degrees which we have surveyed. Fainter than this, the number of Lyman break objects rises rapidly, reaching 5% of the galaxy population at $\mathcal{R} = 25.0$. In the HDF the counts of Lyman break galaxies are higher. This is partially due to the larger volume probed by the color selection technique in the HDF because of the bluer F300W filter. It may also reflect genuine redshift evolution in the galaxy population, however, since the HDF U_{300}–dropout galaxies have lower mean redshifts than do the objects in the ground–based sample, and the total UV luminosity density in galaxies is evidently rising from $z \approx 4$ to 2 (Madau et al. 1996). At $R \approx 26.5$, nearly 1 in 4 galaxies in the HDF is probably at $z \gtrsim 2$.

With a robust technique for identifying large numbers of galaxies in a particular redshift range we may quantify various statistical properties of the population even without complete spectroscopic redshift information. Here I will consider luminosity and color distributions of Lyman break galaxies. Another example is the angular correlation function, which is addressed in the contribution of Giavalisco to this volume.

3.1. *Luminosity functions*

The redshift selection function of our ground–based $U_n G\mathcal{R}$ survey is now well categorized, with more than 400 spectroscopic redshifts measured in many independent survey fields. For a particular color–defined subset of our sample we find that approximately 90% of the galaxies lie at $2.6 < z < 3.4$. The front–to–back "depth" of this redshift range is small, photometrically speaking (i.e. in terms of distance modulus), and thus the counts of Lyman break galaxies, even without confirming redshifts, primarily reflect their intrinsic luminosity distribution.

The physical significance of the "luminosity function" of Lyman break galaxies is different from that of the more familiar optical luminosity functions that have been determined locally and out to $z \approx 1$ from the CFRS, AUTOFIB, CNOC and Hawaii Surveys. By observing $z \approx 3$ galaxies through optical bandpasses we are measuring their luminosities at rest–frame ultraviolet wavelengths of approximately 1500Å. For young galaxies, ultraviolet continuum emission arises mainly from hot, massive stars, modulated by the absorbing effects of dust. In the absence of extinction, the ultraviolet luminosity thus primarily reflects an *instantaneous* property of a galaxy: its star formation rate. The UV luminosity declines rapidly after the cessation of star formation as the O and B stars which produce it burn off the main sequence. In more local galaxy samples, the rest–frame optical light used to define luminosity functions manifests some integral over the past star formation history of a galaxy, and thus better describes its total stellar content. It is therefore most straightforward to interpret the UV luminosity function (UVLF) of Lyman break galaxies as a distribution of star formation rates in the population. The complication, however, is that the effects of extinction on UV emission can potentially be large, and are at present mostly unknown for $z \approx 3$ galaxies. I return to this issue below, considering only the "raw" luminosities here.

Figure 9 presents a composite luminosity distribution for Lyman break galaxies derived from the ground–based and HDF samples. Here I briefly describe the procedures used in constructing this diagram in order to point out some of the inherent uncertainties. A detailed discussion and analysis will be presented in a forthcoming paper (Dickinson et al. 1998).

The overall luminosity distribution has been normalized using data from our ground–based sample. Here the statistics are good thanks to the large number of Lyman break objects and the use of many survey fields to average over local fluctuations, and the redshift selection function is well characterized through extensive spectroscopy. At brighter magnitudes ($\mathcal{R} < 24.5$) there is significant contamination from galactic stars (plus a few

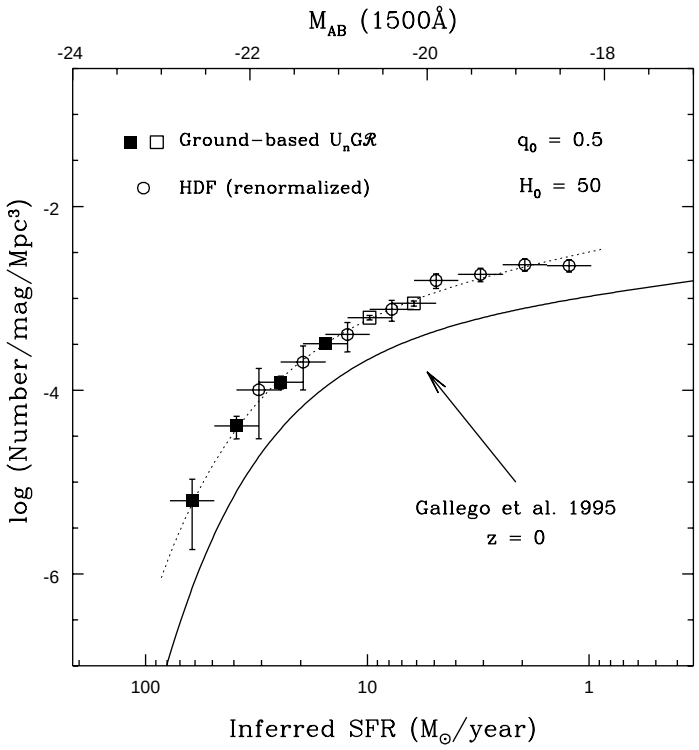

FIGURE 9. The ultraviolet luminosity function of galaxies at $z \approx 3$. Filled and open squares are derived from spectroscopically and photometrically selected galaxies from the ground–based survey, while circles are renormalized counts of objects from the HDF. Absolute magnitudes are computed on the AB system: $M_{AB} = -21$ corresponds to a specific luminosity of 1.1×10^{29} erg s^{-1} Hz^{-1}. The local Hα luminosity function of Gallego et al. (1995) is shown for comparison. Both UV and Hα luminosities are converted to star formation rates (bottom axis) using a Salpeter IMF. See text for discussion.

QSOs). At those magnitudes, therefore, only spectroscopically confirmed galaxies have been used. From $24.5 < \mathcal{R} < 25.5$, the number counts from Figure 9 are used with a small, modeled correction for incompleteness. Spectroscopy has confirmed that the stellar and QSO contamination is very small at these magnitudes. The measured redshift selection function of the ground–based sample is used to normalize the survey volume. The true normalization is probably higher, as I have assumed that the color criteria are 100% efficient at the peak of the selection function ($z = 3.0$). Comparison of our ground–based Lyman break sample in the HDF and the WFPC2 images demonstrates that we do miss some fraction of candidates, even at relatively bright magnitudes, due to photometric confusion with foreground galaxies. For example, 4–555.1, a galaxy at $z = 2.803$ which is one of the brightest Lyman break objects in the HDF (and which is illustrated in figure 1 above) is missed in the ground–based sample due to flux contamination by a foreground elliptical galaxy only $\sim 2''$ away.

The ground–based data, reaching $\mathcal{R} = 25.5$, probes only the relatively bright end of the Lyman break galaxy luminosity function. The HDF offers an opportunity to sample lower luminosities. The difficulty with the HDF sample, however, is that its redshift selection function is quite uncertain; only 24 U_{300}–dropouts have measured redshifts. Moreover, the spectroscopic success rate is probably declining rapidly at $z < 2.3$ due to the lack

of strong spectral features in the wavelength range currently accessible to LRIS. Finally, there is only one HDF and it covers a *very* small region of the sky. As noted above, we now know that Lyman break galaxies are strongly clustered, and thus any single, narrow pencil beam survey will encounter a highly non–random galaxy distribution. This complicates the determination of the redshift selection function, and may compromise any attempt to normalize the luminosity function simply because field–to–field variations cannot be averaged away. The Southern HDF, planned for 1998, will offer a second "realization" of the F300W dropout sample for comparison, but still the total volume surveyed will be small.

In addition, as noted above, the redshift range of the HDF Lyman break galaxies is much broader than that of the ground–based sample, and extends to lower redshifts. HDF U_{300}–dropouts with measured redshifts have $\langle z \rangle \approx 2.7$, but it is likely that the mean redshift of the complete photometrically selected sample is lower still. Madau et al. (1996) suggest that the UV luminosity density of the universe, an integral over the luminosity function, was rising steeply with time at this cosmic epoch, a result derived from the HDF data by comparing numbers of U_{300}– and B_{450}–dropout objects. Therefore the luminosity function itself may have evolved rapidly at these redshifts, providing an additional uncertainty for splicing the ground–based and HDF Lyman break samples together. Also, this broader redshift range means that the photometric "depth" of the survey (in terms of relative distance modulus, front to back) is larger. This complicates the transformation from apparent magnitude distribution to luminosity function, both by blurring the distance modulus conversion and by making k–correction effects somewhat larger.

For the present purposes, I have used the HDF sample mainly to provide an indication of the UVLF slope at faint luminosities. Magnitudes of HDF galaxies are transformed to luminosities assuming $\langle z \rangle = 2.6$. Initially we normalize the survey volume by assuming unit selection efficiency over the range $2 < z < 3.5$. The resulting HDF luminosity function is still higher than the ground–based counts over the range of luminosity overlap. In part this may be due to incompleteness in the ground–based sample, but it is likely that it also manifests to the effect of redshift evolution. Here, the HDF space densities have been scaled downward to match that of the ground–based sample in the luminosity range of overlap. The faintest data points in figure 9 should be regarded with caution, as the sample may suffer as–yet unquantified incompleteness effects at its photometric limits. Thus while the luminosity function appears to be flattening, the apparent slope should be taken as a limit to the true value.

One measure of the distribution of galaxy star formation rates in the local universe is the Hα luminosity function of Gallego et al. (1995). In figure 9, both the $z \approx 3$ UVLF and the Hα measurements at $z \approx 0$ have been converted to star formation rates (SFR) using consistent assumptions of a Salpeter IMF spanning 0.1–125 $M_\odot$ (e.g. Madau et al. 1998; adopting the Kennicutt 1983 conversion for Hα, which assumes a somewhat different IMF, increases the Gallego et al. SFR values by 26%). The SFR distribution at $z = 3$ is strikingly like that measured at $z = 0$, spanning a similar range but with more galaxies per unit volume forming stars at any given rate. The characteristic "L^*" of the $z = 3$ and $z = 0$ SFR distributions are approximately 14 and 10 $M_\odot$ yr^{-1}, respectively, and the faint end slopes are similar.

These similarities may very well be coincidental. No correction has been made for the effects of extinction in the $z = 3$ galaxies (the Gallego et al. Hα data does include an extinction correction). As we will see below, these corrections could be quite significant. Also, the Lyman break luminosity function in figure 9 is plotted for an Einstein–de Sitter cosmology. For an open universe the $z \approx 3$ data translates downward and to the left

relative to the local data, i.e. toward higher luminosities/SFRs but lower space densities. Thus both extinction and cosmology could work in the direction of increasing the typical star formation rates inferred for high redshift galaxies.

The physical state of star formation in the distant galaxies may be quite different than that in the "typical" galaxy actively forming stars in the nearby universe. The sizes of Lyman break galaxies are much smaller than those of ordinary galaxies with similar star formation rates nearby (Giavalisco et al. 1996b, Lowenthal et al. 1997), and their ultraviolet surface brightnesses are much higher, comparable to those of powerful starburst galaxies today (Meurer et al. 1997, Giavalisco et al. 1996a). Again, this suggests that the similarity of the SFR distributions at $z \approx 0$ and 3 may be, to a certain extent, a coincidence.

The integral over the best fit to the UVLF shown in figure 9 gives a comoving 1500Å luminosity density at $z \approx 3$ of 2.1×10^{26} erg s^{-1} Hz^{-1} Mpc^{-3}, corresponding to a star formation density (using the same Salpeter conversion) of $0.026 M_{\odot}$ yr^{-1} Mpc^{-3}, again neglecting any correction for extinction. This value should be regarded as a lower limit because of the possibility of incompleteness in the ground–based sample, although comparison between WFPC2 and ground–based Lyman limit samples suggests such incompleteness is not likely to exceed 30%. Varying the procedure used to construct the data set changes the form of the luminosity function somewhat, and the integrated luminosity density varies from 1.6 to 3.5×10^{26} erg s^{-1} Hz^{-1} Mpc^{-3} because of these systematic changes – this is the dominant uncertainty, significantly exceeding shot noise in the data. As noted above, the integrated luminosity density of the HDF Lyman break galaxies appears to be somewhat larger than that implied from the $z \approx 3$ UVLF which is normalized by the ground–based sample, but uncertainties about the redshift selection function of the HDF sample make it hard to estimate by how much. If real, the excess could be the consequence either of clustering in the small HDF volume or of redshift evolution of the galaxy population, with a larger luminosity density present at the lower redshifts probed by the HDF Lyman break color selection.

3.2. *Colors of high redshift galaxies and measures of extinction*

The preceding discussion of the UVLF of Lyman break galaxies and their star formation explicitly neglected the effect of extinction, which could be strong at ultraviolet wavelengths even if the dust content of these galaxies is relatively small. Indeed we are reasonably sure that these objects do contain some amount of dust, as their Lyman α emission lines are generally much weaker than expected from their UV–derived star formation rates under the assumption of Case B recombination (Steidel et al. 1996a). Lyman α, however, is a resonance line and is easily extinguished with small amounts of dust, so there is little constraint on the dust content from this spectral feature.

A dust–free, star forming galaxy should have a very blue UV continuum – flat in f_{ν} units if star formation has been proceeding for $\gtrsim 10^8$ years, or even bluer for very young starburst populations. If we examine the actual UV spectral slopes of Lyman break galaxies, however, we find that they are mostly redder than flat spectrum in f_{ν}. Figure 10 plots the $G - \mathcal{R}$ color of more than 400 galaxies from our ground–based sample versus redshift. For this color combination knowing the redshift of each galaxy is important because Lyman α forest opacity can effect the flux measured in the G–band, making colors redder at larger redshifts independent of extinction internal to the galaxy. In figure 10, the predicted colors of star–forming galaxies are plotted versus redshift for various amounts of internal extinction. The unreddened models define the blue envelope of the color distribution, with nearly all galaxies being redder than the colors expected from a naked star forming galaxy. This effect is also seen in local starburst galaxy samples

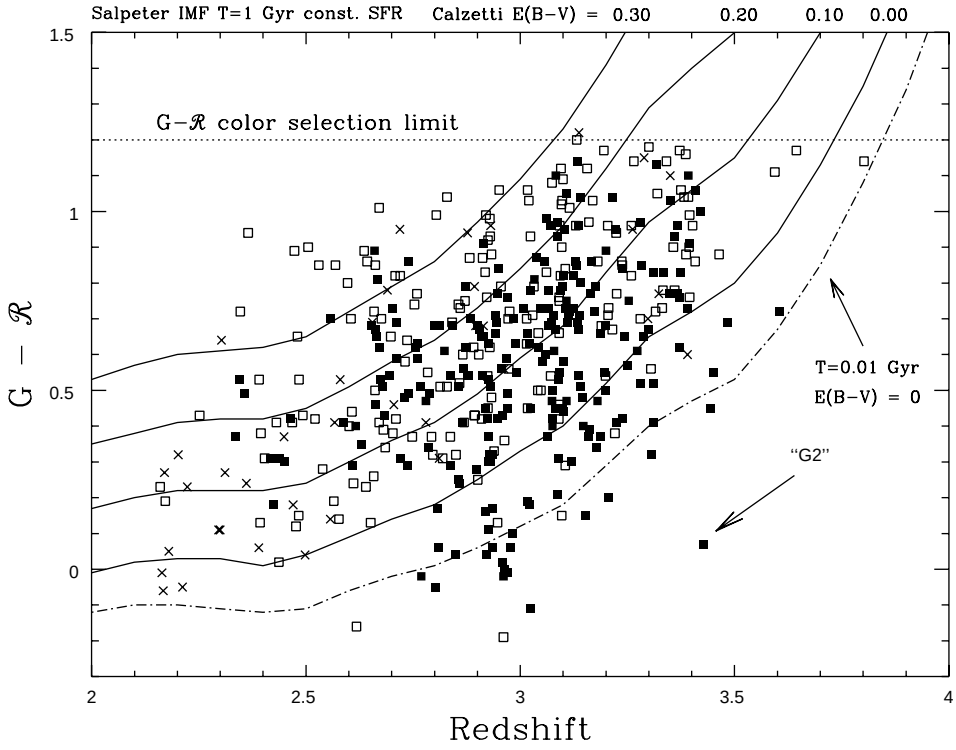

FIGURE 10. $G - R$ color of Lyman break galaxies versus redshift. The various symbol types mark different color–selected subsamples and are not important here. The solid lines show the predicted colors of actively star forming galaxies with various amounts of reddening, using the Calzetti et al. (1994) starburst extinction law. The bluest model track shows an unreddened starburst model with very young (10^7 year) age, i.e. O–star dominated and intrinsically bluer than flat spectrum. The unreddened models define the blue envelope of the color distribution. Some objects which are bluer than the unreddened models have colors affected by strong Lyman α emission lines in the G–band, e.g. the galaxy labeled G2 which is an AGN with very strong line emission.

(e.g. Calzetti et al. 1994), and has been studied in Lyman break galaxies by Meurer et al. (1997). Although for some objects this reddening of the UV spectral slope may be due to ageing of a starburst with a declining star formation rate, it is likely that some or most of the effect is indeed due to extinction.

The difficulty in interpreting UV spectral slopes as a measure of extinction is that the inferred luminosity corrections are tremendously sensitive to the form of the reddening law at UV wavelengths. For local starburst galaxies, an effective attenuation law has been derived which relates UV slope to total extinction (cf. Calzetti et al. 1994; Calzetti 1997). The wavelength dependence of this attenuation law in the near–UV is very "grey," such that a small change in the UV color requires a large change in the total extinction. Varying the UV slope of the extinction law, as well as its normalization, can dramatically change the derived total suppression of UV galaxy luminosities. This is illustrated in figure 11, where I have used the observed colors of Lyman break galaxies in our spectroscopic sample to infer the UV extinction at 1500Å under the assumption of two dust attenuation laws: the SMC extinction curve and the local starburst extinction prescription of Calzetti (1997). Without correction, the star formation rates derived

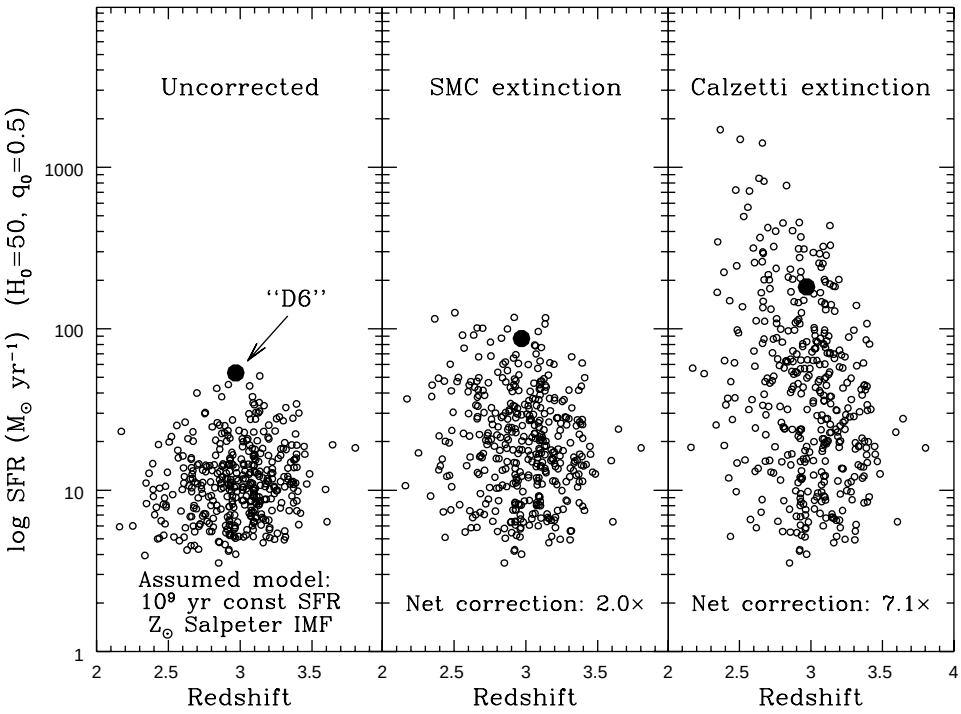

FIGURE 11. Estimates of the effect of extinction on the UV luminosities and derived star formation rates of Lyman break galaxies. The left panel shows computed star formation rates for objects with redshifts in our survey. The most luminous galaxy in the sample, labelled D6, is shown with a large symbol for identification in each panel. In the center and right panels, the $G - R$ color of each object has been used to compute reddening using SMC and Calzetti extinction laws and the appropriate correction has been applied to the star formation rates. At bottom, the net correction to the *observed* population of objects is tabulated.

for the brightest galaxies in our sample are $\sim 50 M_\odot$/year. With SMC extinction, they slightly exceed $100 M_\odot$/year, and the net correction to the overall star formation rate of the Lyman break population is a factor of two. For the starburst attenuation law, the most luminous galaxies approach SFRs of $2000 M_\odot$/year, and the net correction to the *observed* population of galaxies is a factor of 7.1; the actual effect of dust on the global star formation rate would be larger because some intrinsically luminous but reddened galaxies would disappear from of a flux–limited sample. Meurer et al. (1997), using an extinction relation calibrated for local starbursts using correlations between UV spectral slope and far–infrared emission, derive even larger correction factors of $\sim 15\times$ for the Lyman break population, in part due to different assumptions about the spectral slope of the underlying, unreddened continuum.

At present, we have little direct information about the true effects of extinction on the UV luminosities of Lyman break galaxies. While it is plausible that the attenuation law for local starburst galaxies may apply to their high redshift ancestors, the inferred effect on the global UV luminosity is so sensitive to small variations in the extinction law that one wishes for independent data at other wavelengths which could be used to verify star formation rates. In the future, far–infrared measurements of thermally reradiated dust emission in Lyman break galaxies may be possible from SIRTF or WIRE, or with

sub–millimeter observations with the instruments like SCUBA. In the meanwhile, we have begun a program of near–infrared spectroscopy at UKIRT to measure Balmer line emission from Lyman break galaxies, and thus provide an independent measure of their star formation rates which should be less sensitive to extinction. This work is painfully slow compared to optical multislit spectroscopy for measuring redshifts, requiring night–long exposures on one galaxy at a time. Preliminary results are reported by Pettini et al. 1997, and suggest that the star formation rates derived from the Balmer emission may be a few times larger than those inferred from the UV continuum. A much larger sample is needed before we can make secure statements, but at least the problem is addressable by observation. Moreover, the same is now true at low redshift. Recently, Tresse & Maddox (1997) have derived an Hα LF for CFRS galaxies at $z \approx 0.2$, while Treyer et al. (1997) presented a near–UV LF for galaxies at similar redshifts. Comparison of these two LFs, converted to star formation rates, suggests that the UV luminosity density is underestimated of this local sample is suppressed by ~ 1 magnitude, presumably due to the effects of dust.

4. Infrared properties

One difficulty with the HDF WFPC2 data for studying galaxies at $z > 1$ is that their optical rest–frame light is redshifted beyond the WFPC2 filter bandpasses. The WFPC2 images thus provide only an ultraviolet view of the $z > 1$ universe. While this has advantages for detecting and studying active star formation in very distant galaxies, it makes it difficult to compare their properties to those of objects in the nearby universe at familiar rest–frame wavelengths. We may address this problem by collecting data on the nearby universe in the ultraviolet, or by studying HDF galaxies in the near–infrared.

The HDF has been imaged in the infrared by several groups. Len Cowie and colleagues used the CFH and UH 2.2m telescopes to obtain images of the central deep field in J and an "H+K" notched filter, and have imaged a much wider surrounding region ($9' \times 9'$) to shallower depths. Hogg et al. (1997) used the NIRC camera on Keck to obtain deep images of two small ($\approx 40'' \times 40''$) fields within the HDF, and the Caltech group has also covered a wider surrounding region with the Palomar 60–inch. My collaborators and I imaged the central HDF using IRIM on the KPNO Mayall 4m telescope over the course of ten nights. The field of view of IRIM is well matched to that of the WFPC2, providing easy coverage of the complete HDF. Data was collected in the J, H and K bands, and reach formal 5σ limiting magnitudes in a $2''$ diameter aperture of $J = 23.5$, $H = 22.3$ and $K = 21.9$. These images are available to the community, and have been used by several groups presenting results at this symposium. For further information and access to the data, please see `http://www.stsci.edu/ftp/science/hdf/clearinghouse/irim/irim_hdf.html`.

A complete discussion of the infrared properties of galaxies in the HDF is beyond the scope of this presentation. Here I restrict my attention to a few simple color properties of $z > 2$ Lyman break selected galaxies. Although WFPC2 optical photometry in this paper is presented in AB units, I will use standard (Vega–normalized) infrared magnitudes in the discussion that follows. For reference, the approximate conversion to AB units for the K_S bandpass used for the IRIM observations is $K_{AB} = K_{\rm Vega} + 1.86$.

4.1. *Colors and luminosities*

Figure 12 plots $V_{606} - K$ colors for galaxies in the HDF with spectroscopically confirmed redshifts (plus a few stars). At $0 < z \lesssim 1$, galaxy colors are nicely bounded by the range expected for star forming "irregulars" to old ellipticals. The "red envelope" of

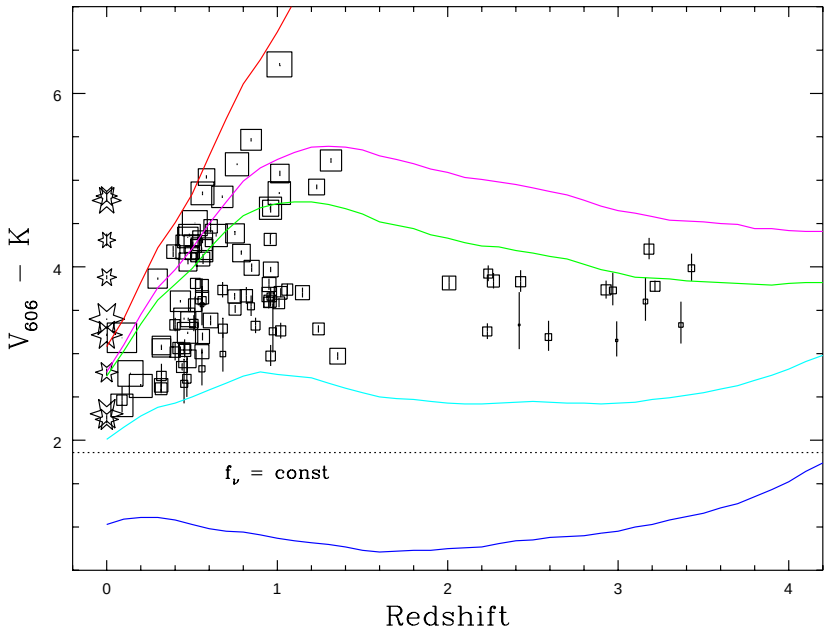

FIGURE 12. Color versus redshift for galaxies with spectroscopic identifications in the HDF. The symbol sizes scale inversely with apparent K magnitude; star–shaped symbols at $z = 0$ are known galactic stars. The solid lines are *unevolving* tracks of k–corrected color vs. redshift for various model galaxy spectral energy distributions designed to span the range (reddest to bluest) from old ellipticals to actively star forming irregulars. The bluest model track, with $V_{606} - K \approx 1$ at most redshifts, is an extremely young (age = 10^7 year) unreddened starburst. There are no spectroscopically observed galaxies in the HDF which approach this color.

galaxies at $z \approx 1$ is only slightly bluer than are giant elliptical galaxies in the local universe. (Indeed, perhaps the most luminous galaxy in the HDF at rest–frame optical wavelengths is a giant elliptical at $z = 1.012$.) Figure 13 shows shows the colors of nearly all optically selected U_{300}–dropout galaxies in the HDF brighter than $V_{606} = 27$. (A few have been excluded due to photometric confusion with other objects in the near–IR data). Most Lyman break galaxies with $V_{606} < 25.5$ are detected in the infrared images. Beyond that magnitude there is increasing incompleteness due to the limited depth of the IR data.

Lyman break galaxies mostly have colors in the range $2.5 < V_{606} - K < 4.5$ (although we cannot rule out that some of the fainter objects are intrinsically bluer). As can be seen from the model tracks in figure 12 these colors (shifted to the UV–optical rest frame) would be normal for actively star forming spirals (Sb–Sc) in the local universe. They are all much redder (as indeed are all HDF galaxies) than the expected colors of an extremely young, unreddened starburst spectrum – indeed, there are few faint galaxies anywhere in the universe which are as blue or bluer than a flat (f_ν) spectrum over a long (optical–IR) wavelength baseline. The observed color does not, of course, tell us *why* the Lyman break galaxies have these colors; the effects of dust extinction on the rest–frame UV emission could have a significant impact on the observed colors (see previous section). The typical ("L^*" from figure 9) Lyman break galaxy at $z \approx 3$ has $K = 21.5 \pm 1$, corresponding to rest–frame $M_V = -22 \pm 1$ for $H_0 = 50$, $q_0 = 0.5$, i.e. similar to L_V^* locally.

Figure 14 shows a color–magnitude diagram for a K–selected sample of objects in the

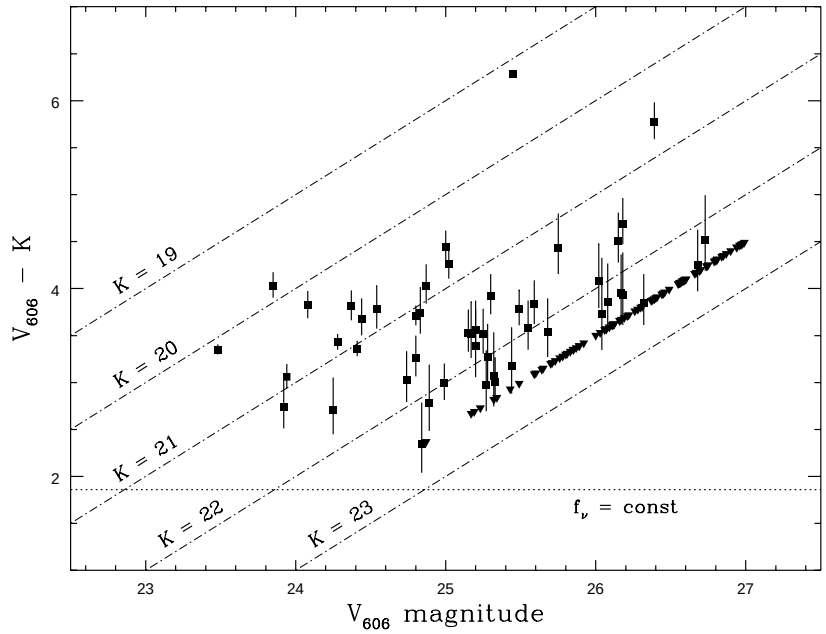

FIGURE 13. $V_{606} - K$ colors of U_{300} Lyman break selected galaxies in the HDF. Note that only a small subset of these galaxies have spectroscopic redshifts. Objects with $K > 22.5$ (i.e. beyond the robust detection limit of our IR data) are plotted as lower limits (triangles) at that magnitude.

HDF. Different symbol types code the objects as U_{300}–dropout Lyman break objects (with or without spectroscopic confirmation), galaxies with spectroscopically measured $z < 2$, stars, or unobserved objects (but which presumably mostly have $z < 2$, since they do not qualify as Lyman break candidates). The optical–IR colors of the Lyman break galaxies are quite typical for the general population of faint galaxies in the HDF.

Two galaxies in figures 13 and 14 have significantly redder optical–IR colors ($V_{606} - K$) than the majority of Lyman break objects. Although they both satisfy the color selection criteria defined in §2.1, it is not certain that these are also at $z > 2$. In addition to their relatively bright infrared magnitudes, they are also much redder in $V_{606} - I_{814}$ than the majority of Lyman break galaxies ($V_{606} - I_{814} \approx 0.7$ to 1.0 – compare with figure 4), and their overall spectral energy distributions are quite different than those of the known $z > 2$ galaxies in the HDF. At present, neither object has a spectroscopic redshift; future observations should establish whether these are unusually red and luminous members of the Lyman break population or interlopers into the color selected sample from lower redshifts.

4.2. *Morphologies*

Existing ground–based near–IR images of Lyman break galaxies in the HDF and elsewhere are mostly inadequate for answering questions about the rest–frame optical morphologies of these objects. Our KPNO IRIM images of the HDF, for example, have a resolution of $\approx 1''$, much larger than the typical scale lengths associated with the rest–frame UV light seen in WFPC2 images (Giavalisco et al. 1996b). However, a few simple conclusions can be drawn from the existing data. In general, the centroid position of the infrared emission is spatially coincident with that of the optical images, suggesting that

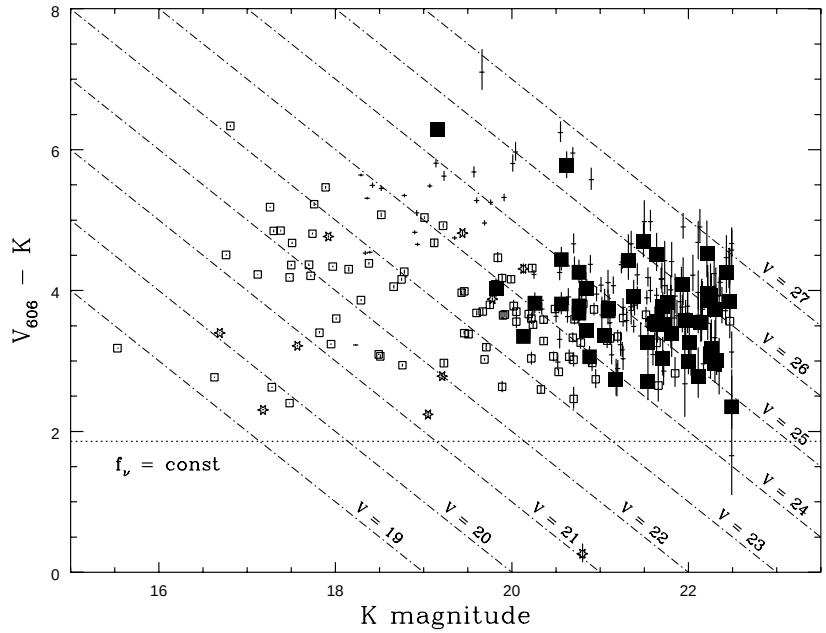

FIGURE 14. $V_{606} - K$ color versus K magnitude for objects with $K < 22.5$ and $V_{606} < 27.0$ in the HDF. Lyman break selected galaxies are plotted as filled boxes. Galaxies with spectroscopic redshifts $0 < z < 2$ are plotted as unfilled boxes; galactic stars are shown as star symbols. Objects without spectroscopic observations are plotted as small crosses.

in most cases there is no substantial "displacement" between the dominant sources of rest–frame UV and optical luminosity in these objects. In the HDF, however, there is one spectacular exception found in galaxy 2–585.1, the $z = 2.01$ object whose redshift was serendipitously measured by Elston et al. (see §2.2 above). The WFPC2 images of this galaxy show a chain–like assembly of blobs $\sim 3''$ long, making it rather unusual among the Lyman break objects, which are mostly quite compact. The near–IR emission is spatially extended, with its peak/centroid located just beyond one end of the "chain," coincident with diffuse optical emission seen in the WFPC2 images. In this object it appears that spatially segregated stellar populations and/or extinction are affecting the observed morphology – the high surface brightness, star forming "blobs" of the chain structure protrude radially outward from a larger, red host galaxy.

5. Summary

In this presentation I have tried to use HDF data to illustrate the ways in which multi–color photometry can be used first to select galaxies at high redshift and then to learn something about their intrinsic properties. The great depth of the HDF and the precision of its photometry makes it ideal for illustrating and applying the Lyman break color selection technique: cf. the remarkable prominence of the high redshift "plume" in figures 2 and 4. By $V_{606} = 26.5$, nearly 1 in 4 HDF galaxies is a Lyman break candidate and thus is likely to be at $z > 2$. Spectroscopy of HDF galaxies at all redshifts has proceeded at a remarkable pace. After only two observing seasons, the central HDF is almost certainly the piece of celestial real estate with the highest surface density of measured galaxy redshifts (now $\approx 24/\mathrm{arcmin}^2$, of which $\sim$20% are at $z > 2$).

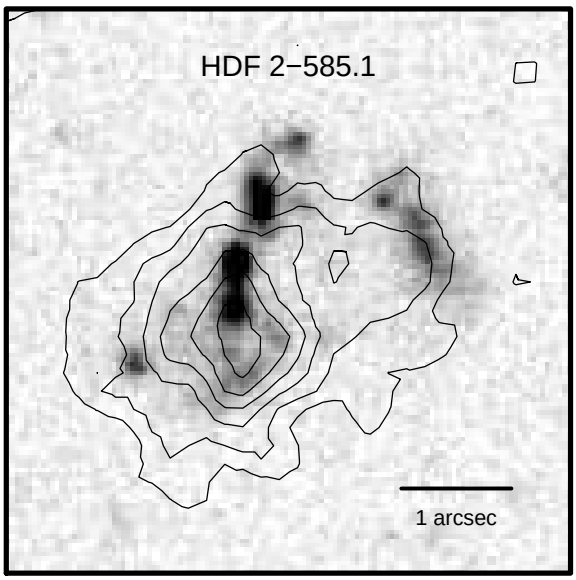

FIGURE 15. V_{606} WFPC2 image of the $z = 2.01$ Lyman break galaxy 2–585.1 (greyscale) overlaid with contours from the ground–based infrared image. Although the $\approx 1''$ resolution of the ground–based image does not allow morphological details to be discerned, there is a clear spatial offset between the peak of the IR emission and the brightest structures visible in the rest–frame UV. The object toward the upper right is not a Lyman break candidate and thus is unlikely to be related to 2–585.1.

The distribution of ultraviolet luminosities of $z \approx 3$ galaxies, converted to star formation rates using a simple prescription, spans a similar range to that of galaxies in the local universe. Schechter function fits give a characteristic 1500Å specific luminosity of $M_{AB} \approx -21$ (for $H_0 = 50$, $q_0 = 0.5$), corresponding to a star formation rate of $\sim 14 M_\odot$/year. Very few Lyman break galaxies have "raw" SFRs $> 50 M_\odot$/year. If these measurements are taken at face value, these objects cannot produce the total stellar mass of $\sim L^*$ galaxies in short timescales as traditional "monolithic" formation scenarios for elliptical galaxies would require. This, then, would suggest that massive galaxy formation takes place either at still higher redshifts where we have yet to look, or proceeds by the hierarchical assembly of smaller objects as expected in theories such as CDM. However, the possible extinction corrections to the UV luminosities of Lyman break galaxies are highly uncertain and could be quite large. Their UV colors are redder than expected from spectral models of "naked" star forming galaxies, a fact which could easily be explained by the presence of dust. The derived extinction corrections based on these colors, however, are extremely sensitive to the form of the extinction law in the ultraviolet, and can range from factors of 2 to > 7. New observations in the infrared, and eventually at far–IR and sub–millimeter wavelengths, will provide an independent measure of star formation rates which can be useful for addressing this question.

Characteristic rest–frame optical luminosities of Lyman break galaxies, as measured from infrared photometry, are $M_V = -22$. Their UV–optical rest–frame colors galaxies span a range which would be typical for normal spirals in the nearby universe. Detailed morphological study of $z \approx 3$ galaxies at rest–frame optical wavelengths must await observations with NICMOS, which will take place in 1997–1998.

Although Lyman break color selection is a simple technique compared to more sophisticated photometric redshift methods, it has the virtue of being relatively model

independent and easy to apply and understand. Like all such methods, however, its utility depends strongly on the degree to which it is tested and calibrated by follow–up spectroscopy, which requires substantial effort on large ground–based telescopes. With hundreds of Lyman break redshifts in hand, we can begin to carry out fairly sophisticated analyses of the luminosity function, clustering, and other properties of galaxies at $z \approx 3$. For the HDF, despite the impressive observing efforts to date, we are unlikely ever to succeed in collecting hundreds of redshifts for $z > 2$ galaxies with existing telescopes and instrumentation. However, we may take advantage of the insights gained from studying the Lyman break galaxy population in non–HDF data sets to aid interpretation of the HDF objects, and thus to use the HDF to push the method to different flux and redshift limits.

Regardless of how much we learn about high redshift galaxies in the HDF, we must remind ourselves of what a small volume the HDF probes. The entire comoving volume over which U_{300}–dropouts have been found in the HDF, $2 < z < 3.5$, is only $18000 h_{50}^{-3}$ Mpc^3 for $q_0 = 0.5$. Locally, that would correspond to a sphere with radius $16.2 h_{50}^{-1}$ Mpc – not even reaching the Virgo cluster! We must therefore be cautious about how representative HDF galaxies are in any statistical sense, particularly in light of recent evidence for strong clustering at $z > 2$. The pencil–beam geometry of the HDF volume ensures that it will traverse a wider range of large scale structures than would the corresponding 14.2 Mpc radius sphere locally, but such a geometry brings its own complications for some applications. For example, clustering may introduce large fluctuations in $N(z)$ which can seriously complicate analyses of the redshift evolution of galaxy properties, global luminosity density, etc. It is therefore risky to extrapolate too far from the HDF to the properties of galaxies in the high redshift universe as a whole. Ultimately, however, the insights gathered from the HDF, when calibrated with data from ground–based, large–volume surveys, should provide a powerful means of understanding the early stages in the evolution of normal galaxies.

I would like to extend special thanks to my collaborators Chuck Steidel, Mauro Giavalisco, Max Pettini, Kurt Adelberger, and Mindy Kellogg, for endlessly interesting discussions, much hard work, and for allowing me to present materials in advance of publication. The same thanks also go to Adam Stanford, Peter Eisenhardt, Richard Elston, and Matt Bershady for their collaboration on the KPNO infrared imaging program. Finally, I would also like to thank my colleagues at STScI from the HDF Team, and the editors of this volume for their considerable patience.

REFERENCES

Calzetti, D., Kinney, A.L., & Storchi–Bergmann, T., 1994, ApJ, 429, 582.

Calzetti, D., 1997, in *The Ultraviolet Universe at Low and High Redshift,* ed. W. Waller (Woodbury: AIP Press), in press (astro-ph/9706121).

Cohen, J.G., Cowie, L.L., Hogg, D.W., Songaila, A., Blandford, R., Hu, E.M., & Shopbell, P., 1996, ApJ, 471, L5.

Colley, W.M., Rhoads, J.E., Ostriker, J.P., & Spergel, D.N., 1996, ApJ, 473, L63.

Gallego, J., Zamorano, J., Aragón–Salamanca, A., & Rego, M., 1995, ApJ, 455, L1.

Franx, M., Illingworth, G., Kelson, D.D., Van Dokkum, P.G., & Tran, K., 1997, ApJ, 486, L75.

Giavalisco, M., Livio, M., Bohlin, R.C., Macchetto, F.D., & Stecher, T.P., 1996a, AJ, 112, 369.

Giavalisco, M., Steidel, C.C., & Macchetto, F.D., 1996b, ApJ, 470, 189.

Giavalisco, M., Steidel, C.C., Adelberger, K.L., Dickinson, M., Pettini, M., & Kellogg, M., 1998, ApJ, submitted.

Guhathakurta, P., Tyson, J.A., & Majewski, S.R., 1990, ApJ, 357, L9.

Hogg, D.W., Blandford, R., Kundic, T., Fassnacht, C.D., & Malhotra, S., 1996, ApJ, 467, L73.

Hogg, D.W., Neugebauer, G., Armus, L., Matthews, K., Pahre, M.A., Soifer, B.T., & Weinberger, A.J., 1997, AJ, 113, 2338.

Kennicutt, R.C., 1983, ApJ, 272, 54.

Lowenthal, J.D., Koo, D.C., Guzman, R., Gallego, J., Phillips, A.C., Faber, S.M., Vogt, N.P., Illingworth, G.D., & Gronwall, C., 1997, ApJ, 481, 673.

Madau, P., 1995, ApJ, 441, 18.

Madau, P., Ferguson, H.C., Dickinson, M., Giavalisco, M., Steidel, C.C., & Fruchter, A., 1996, MNRAS, 283, 1388.

Madau, P., Pozzetti, L, & Dickinson, M., 1998, ApJ, in press (astro-ph/9708220).

Meurer, G.R., Heckman, T.M., Lehnert, M.D., Leitherer, C., & Lowenthal, J., 1997, AJ, 114, 54.

Pettini, M., Steidel, C.C., Dickinson, M., Kellogg, M., Giavalisco, M., & Adelberger, K.L., 1997, in *The Ultraviolet Universe at Low and High Redshift,* ed. W. Waller (Woodbury: AIP Press), in press (astro-ph/9707200).

Songaila, A., Cowie, L.L., & Lilly, S.J., 1990, ApJ, 348, 371.

Steidel, C.C., & Hamilton, D., 1992, AJ, 104, 941.

Steidel, C.C., Pettini, M., & Hamilton, D., AJ, 110, 2519.

Steidel, C.C., Giavalisco, M., Pettini, M., Dickinson, M., & Adelberger, K.L., 1996a, ApJ, 462, L17.

Steidel, C.C., Giavalisco, M., Dickinson, M., & Adelberger, K.L., 1996b, AJ, 112, 352.

Steidel, C.C., Adelberger, K.L., Dickinson, M., Giavalisco, M., Pettini, M., & Kellogg, M., 1998, ApJ, 492, 428.

Tresse, L., & Maddox, S.J., 1997, ApJ, in press (astro-ph/9709240).

Treyer, M.A., Ellis, R.S., Milliard, B., & Donas, J., 1997, in *The Ultraviolet Universe at Low and High Redshift,* ed. W. Waller (Woodbury: AIP Press), in press (astro-ph/9706223).

Warren, S.J., Hewitt, P.C., Irwin, M.J., McMahon, R.G., Bridgeland, M.T., Bunclark, P.S., & Kibblewhite, E.J., 1987, Nature, 325, 131.

Williams, R.E., et al. 1996, AJ, 112, 1335.

Zepf, S.E., Moustakas, L.A., & Davis, M., 1997, ApJ, 474, L1.